JACS
JOURNAL OF THE AMERICAN CHEMICAL SOCIETY
Article
pubs.acs.org/JACS

Cell-Penetrating Hyperbranched Polyprodrug Amphiphiles for Synergistic Reductive Milieu-Triggered Drug Release and Enhanced Magnetic Resonance Signals

Xianglong Hu,[†,‡] Guhuan Liu,[†] Yang Li,[†] Xiaorui Wang,[†] and Shiyong Liu*[,†]

[†]CAS Key Laboratory of Soft Matter Chemistry, Hefei National Laboratory for Physical Sciences at the Microscale, Collaborative Innovation Center of Chemistry for Energy Materials, Department of Polymer Science and Engineering, University of Science and Technology of China, Hefei, Anhui 230026, China

[‡]Ministry of Education Key Laboratory of Laser Life Science, Institute of Laser Life Science, College of Biophotonics, South China Normal University, Guangzhou 510631, China

Supporting Information

ABSTRACT: The rational design of theranostic nanoparticles exhibiting synergistic turn-on of therapeutic potency and enhanced diagnostic imaging in response to tumor milieu is critical for efficient personalized cancer chemotherapy. We herein fabricate self-reporting theranostic drug nanocarriers based on hyperbranched polyprodrug amphiphiles (**hPAs**) consisting of hyperbranched cores conjugated with reduction-activatable camptothecin prodrugs and magnetic resonance (MR) imaging contrast agent (Gd complex), and hydrophilic coronas functionalized with guanidine residues. Upon cellular internalization, reductive milieu-actuated release of anticancer drug in the active form, activation of therapeutic efficacy (>70-fold enhancement in cytotoxicity), and turn-on of MR imaging (~9.6-fold increase in T_1 relaxivity) were simultaneously achieved in the simulated cytosol milieu. In addition, guanidine-decorated **hPAs** exhibited extended blood circulation with a half-life up to ~9.8 h and excellent tumor cell penetration potency. The hyperbranched chain topology thus provides a novel theranostic polyprodrug platform for synergistic imaging/chemotherapy and enhanced tumor uptake.

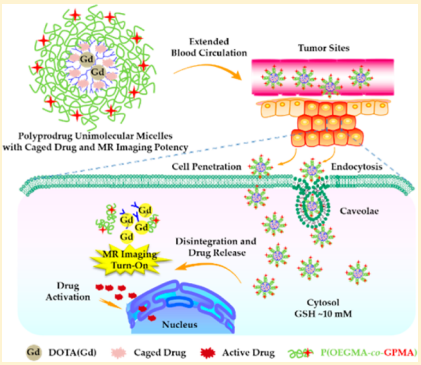

INTRODUCTION

With the rapid progress of nanomedicine, polymeric drug nanocarriers have held great promise to address intrinsic limitations associated with small molecule anticancer drugs, such as poor water solubility, undesired pharmacokinetics, and severe side effects.[1] Up to now, synthetic polymers with various architectures, including linear, miktoarm, star, and branched polymers and dendrimers as well as their supramolecular assemblies (e.g., micelles and vesicles), have been explored as scaffolds for physical encapsulation or covalent conjugation of chemotherapeutic drugs, aiming to achieve enhanced water solubility, high loading capacity, sustained or triggered release, and site-specific accumulation within tumor tissues.[2] Among these, branched and hyperbranched polymers lead to drastic increase in blood circulation duration due to elevated chain flexibility and deformability, as compared with their linear counterparts.[3] However, although PEGylated poly(L-lysine) (PLL) dendrimers conjugated with camptothecin (CPT) anticancer drug possessed extended blood circulation, this system exhibited undefined drug metabolism pathways, uncontrolled release profile, and relatively low drug loadings. These major issues remain to be solved for the optimum design of polymeric drug delivery systems.[4]

On the other hand, polymeric drug delivery systems integrated with diagnostic imaging functions have emerged as an important strategy for more effective personalized treatment.[5] These theranostic platforms allow for concurrent monitoring and treatment at the lesion site.[6] As one of the most powerful and clinically applied medical diagnostic techniques, magnetic resonance (MR) imaging is noninvasive and possesses high spatiotemporal resolution and imaging sensitivity.[7] Accordingly, MR imaging contrast agents and therapeutic drugs were co-loaded into a polymeric delivery matrix with varying chain topologies to achieve integrated theranostic functions.[8]

Concerning chain architectural effects, previous reports revealed distinct advantages in MR relaxivity modulation for macromolecular ligands with nonlinear chain topologies compared to their linear and small molecule counterparts.[8g] Furthermore, polymeric systems with MR imaging contrast effects being responsive to external pathological milieu are highly desired due to advantages such as low background signals and enhanced sensitivity, but this emerging field has been far less explored.[9] In the context of polymeric theranostic systems, it has remained a considerable challenge to concurrently synchronize the triggered drug release process with prominent changes in MR imaging signals.[10] Thus, the

Received: October 21, 2014
Published: December 12, 2014

dx.doi.org/10.1021/ja5105848 | J. Am. Chem. Soc. 2015, 137, 362−368

integrated MR imaging mode can simultaneously monitor both drug release and therapeutic feedback.

In view of our previous works concerning linear polyprodrug amphiphiles[11] as well as stimuli-switchable MR and fluorescence dual imaging polymeric nanocarriers,[8c] and given that branched/hyperbranched polymer-drug conjugates possess extended blood circulation, we propose the concept of theranostic hyperbranched polyprodrug amphiphiles (**hPAs**) with hydrophobic cores polymerized from CPT prodrug monomer and covalently tethered with Gd complex as MR imaging contrast agents (Scheme 1). The extremely hydrophobic CPT prodrugs located within hyperbranched cores can avoid interactions between CPT and blood components to optimize pharmacokinetics and preclude CPT from undesired conversion into the inactive carboxylate form.[12] The polyprodrug strategy possesses combined advantages such as facile preparation, high drug loading, caged drug activity, and triggered release of drugs in the active form.[11,13] The hyperbranched polyprodrug cores serve as the embedding matrix for T_1-type MR contrast agents to weaken MR background signals. Herein, we report the fabrication and theranostic functions of **hPAs** including *h*-P(CPTM-*co*-DOTA(Gd))-*b*-P(OEGMA-*co*-GPMA) (**hPA-2**), where CPTM is the polymerizable monomer of CPT prodrug, OEGMA is oligo(ethylene glycol) monomethyl ether methacrylate, and GPMA is guanidinopropyl methacrylamide. In aqueous media, **hPA-2** existed as structurally stable unimolecular micelles with hydrophilic coronas covalently modified with guanidine moieties. Under physiological condition, the CPT drug was caged and the therapeutic efficacy was silenced. For Gd(III) moieties conjugated onto hyperbranched cores, the hydrophobic polyprodrug matrix will greatly hinder the exchange of water molecules surrounding Gd complex, thus reducing background MR signals during blood circulation. Upon tumor cell internalization, CPT release from **hPA-2** will be triggered by the reductive milieu (e.g., cytosol GSH ~10 mM), resulting in the boosting of chemotherapeutic efficacy. Synchronously, MR contrast performance can be enhanced (~9.6-fold) due to the hydrophobic-to-hydrophilic transition of hyperbranched cores (Scheme 2B). In addition, guanidine moieties within coronas and the hyperbranched topology endow **hPA-2** with tumor cell penetration potency, but with no loss of the extended blood circulation feature.

Scheme 1. Schematic Illustration of Polyprodrug Unimolecular Micelles with Hyperbranched Cores Conjugated with DOTA(Gd) and Reductive Milieu-Cleavable Camptothecin Prodrugs and Hydrophilic Coronas Functionalized with Guanidine Residues[a]

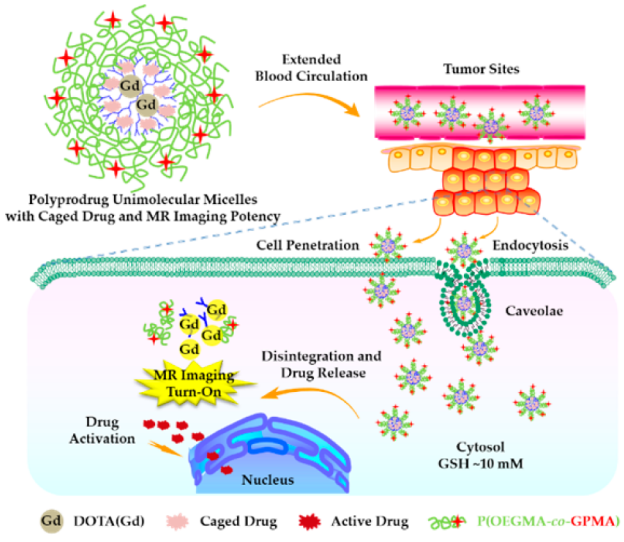

[a]Structurally stable theranostic unimolecular micelles with prolonged blood circulation and cellular internalization features exhibit reductive cytosol milieu-triggered disintegration of hyperbranched cores and release of active CPT drugs, accompanied with distinct turn-on of magnetic resonance imaging signals due to hydrophobic-to-hydrophilic transition of the local milieu surrounding the DOTA(Gd) complex.

Scheme 2. (A) Reaction Schemes Employed for the Synthesis of Hyperbranched Polyprodrug Amphiphiles, *h*-P(CPTM-*co*-DOTA(Gd))-*b*-P(OEGMA-*co*-GPMA) (hPA-2), and (B) Proposed Mechanism of Reductively Activated CPT Parent Drug Release in Cytosol Milieu from Hyperbranched Polyprodrug Cores and Concurrent Hydrophobic–Hydrophilic Transition of the Local Milieu Surrounding the Gd Complex

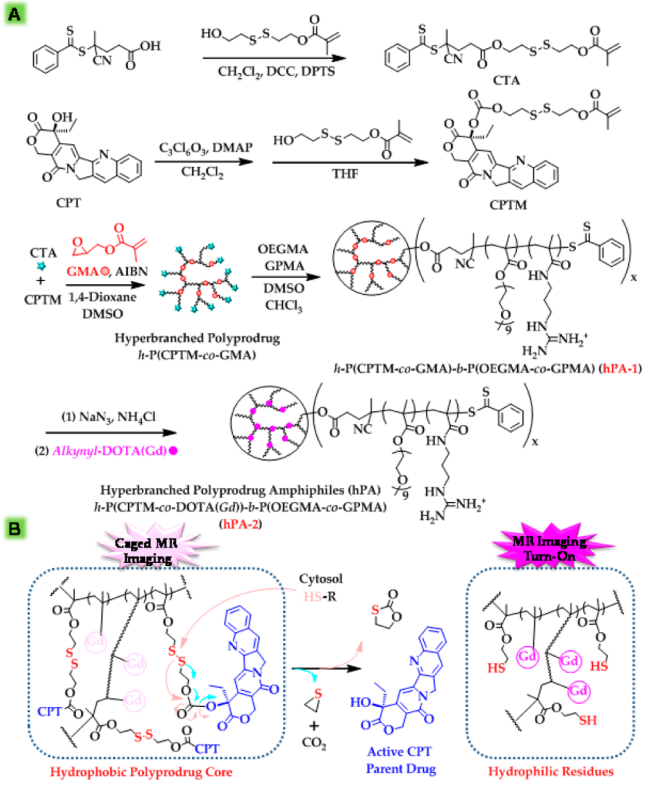

RESULTS AND DISCUSSION

Hyperbranched polyprodrug *h*-P(CPTM-*co*-GMA) cores were synthesized at first via inimer-type reversible addition–fragmentation chain transfer (RAFT) copolymerization of CPTM and glycidyl methacrylate (GMA); the subsequent RAFT copolymerization of OEGMA and GPMA using *h*-P(CPTM-*co*-GMA) macroRAFT agent afforded *h*-P(CPTM-*co*-GMA)-*b*-P(OEGMA-*co*-GPMA), **hPA-1**; upon further azidation of GMA and click reaction with *alkynyl*-functionalized DOTA(Gd), theranostic polyprodrug **hPA-2** with a relatively high drug loading content (~17.3 wt%) was obtained (Scheme 2A). The prodrug monomer (CPTM) containing a reduction-

dx.doi.org/10.1021/ja5105848 | J. Am. Chem. Soc. 2015, 137, 362–368

cleavable disulfide linker and a carbonate moiety, both contributing to the self-immolative cleavage feature,[14] was synthesized in high yield.[11] The RAFT agent containing a polymerizable methacrylate moiety (inimer, CTA) was utilized to generate hyperbranched cores through copolymerization with CPTM and GMA.[15] The hyperbranched polyprodrug was denoted as *h*-P(CPTM$_{0.83}$-*co*-GMA$_{0.17}$)$_{120}$ and shortened as *h*-P(CPTM-*co*-GMA) (Supporting Information, Figures S1a and S2a).

After that, *h*-P(CPTM-*co*-GMA) was employed as a macroRAFT agent to mediate the copolymerization of OEGMA and GPMA to grow hydrophilic corona chains (Scheme 2A). The appearance of new resonance signals characteristic of OEGMA and GPMA moieties in the ^{1}H NMR spectrum confirmed the successful polymerization (Supporting Information, Figure S1b). Guanidine-decorated *h*-P(CPTM-*co*-GMA)-*b*-P(OEGMA-*co*-GPMA), **hPA-1**, was further characterized by gel permeation chromatography in combination with multi-angle light scattering (GPC/MALS) (Figure S2c and Table 1). Subsequently, the azidation reaction

Table 1. Structural Parameters of Polymer Precursors and Hyperbranched Polyprodrug Amphiphiles

entry	samples	$M_{n,NMR}$[a] (kDa)	$M_{n,GPC}$[c] (kDa)	M_w/M_n[c]	DLC[d] (%)
/	*h*-P(CPTM-*co*-GMA)	62.3	41.7	1.39	55.7
hPA-1	*h*-P(CPTM-*co*-GMA)-*b*-P(OEGMA-*co*-GPMA)	187.4	176	1.28	18.5
hPA-2	*h*-P(CPTM-*co*-DOTA(Gd))-*b*-P(OEGMA-*co*-GPMA)	–[b]	213	1.29	17.3
/	*h*-P(CPTM-*co*-GMA)-*b*-POEGMA	185.8	165	1.30	18.7
hPA-3	*h*-P(CPTM-*co*-DOTA(Gd))-*b*-POEGMA	–[b]	207	1.31	17.5

[a]Number-average molecular weights determined by ^{1}H NMR. [b]Gd-containing polymers (**hPA-2** and **hPA-3**) cannot be analyzed by ^{1}H NMR. [c]Molecular weights and molecular weight distributions, M_w/M_n, were evaluated by GPC/MALS. [d]Drug loading content (DLC) was calculated as the ratio of conjugated drug weight to the weight of hyperbranched polyprodrug amphiphiles.

of **hPA-1** was conducted and the formation of *h*-P(CPTM-*co*-GMA-N_3)-*b*-P(OEGMA-*co*-GPMA) was evidenced by the characteristic infrared absorption band of azide at ~2100 cm^{-1} (Supporting Information, Figure S3b). Finally, the click reaction with *alkynyl*-DOTA(Gd) afforded **hPA-2**. FT-IR spectrum further verified quantitative azide transformation and complete removal of excess *alkynyl*-DOTA(Gd) (Supporting Information, Figure S3c). In addition, GPC analysis of **hPA-2** revealed an obvious shift to the higher MW side compared with that of **hPA-1** (Supporting Information, Figure S2e vs S2c). The Gd content in **hPA-2** was determined to be ~1.6 wt % by ICP-AES measurements. Following similar procedures, guanidine-free polyprodrug **hPA-3**, *h*-P(CPTM-*co*-DOTA-(Gd))-*b*-POEGMA, was also synthesized (Supporting Information, Figures S1c and S2d, and Table 1).

For the hyperbranched star copolymer **hPA-2**, it contains caged CPT prodrugs and conjugated MR contrast agents in the hydrophobic cores, as well as guanidine-decorated hydrophilic coronas (Schemes 1 and 2). The multi- or uni-molecular aggregation behavior of **hPA-2** in aqueous media was then explored via the conventional cosolvent (THF) approach. TEM observation revealed the presence of fairly monodisperse and spherical nanoparticles with an average diameter of ~25 nm (Figure 1A). Moreover, dynamic light scattering (DLS)

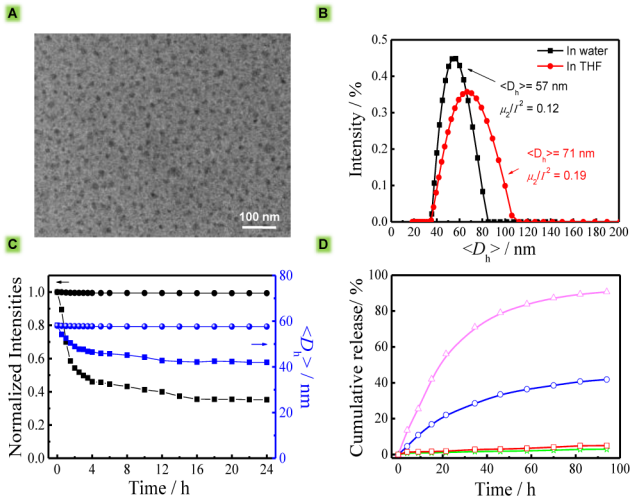

Figure 1. (A) TEM image obtained by drying the aqueous dispersion of **hPA-2** polyprodrug unimolecular micelles. (B) Hydrodynamic diameter distributions, <D_h>, recorded for **hPA-2** in water and THF, respectively. (C) Time-dependent scattered light intensities and intensity-average hydrodynamic diameters, <D_h>, determined by DLS for 0.1 g/L aqueous solution of **hPA-2** upon treating with (●) 0 mM DTT and (■) 10 mM DTT in PBS buffer (pH 7.4 and 37 °C). (D) CPT release profiles recorded for **hPA-2** solution in PBS buffer upon treating with DTT of varying concentrations: (☆) 0 mM DTT, (□) 2 μM DTT, (○) 5 mM DTT, and (△) 10 mM DTT.

measurements revealed that the intensity-average hydrodynamic diameter of **hPA-2** increased from ~57 nm in water to ~71 nm in THF, which should be ascribed to the swelling of hyperbranched polyprodrug cores (Figure 1B). Based on the above results, we concluded that **hPA-2** existed as covalently interconnected unimolecular micelles in aqueous media.[16]

Reductively activated CPT release was initiated by disulfide bond cleavage, and the released thiol was expected to cyclize into the proximate carbonyl group within the self-immolative linker, affording CPT parent drug and cyclic thiocarbonate (Scheme 2B);[11,17] meanwhile, in an alternative mechanism possibly combined with the former one, the sequential release of thiirane and carbon dioxide also led to CPT release.[18] In consideration of disulfide-associated self-immolative linkages in CPTM prodrug moieties within hyperbranched cores, DLS was employed to monitor reduction-responsive degradation of **hPA-2** under simulated tumor cytosol reductive milieu (Figure 1C). Upon incubation with 10 mM DTT, scattered light intensity decreased drastically during the initial 6 h, then further decreased to ~34% at 24 h; meanwhile, $\langle D_h \rangle$ decreased from ~56 nm to ~42 nm in the same period. However, in the absence of DTT, both size and scattered light intensity kept almost unchanged, exhibiting excellent stability under non-reductive physiological conditions. The structural stability of **hPA-2** polyprodrug unimolecular micelles is thus a great advantage compared to conventional block copolymer micelles or vesicles. CPT release profiles of **hPA-2** were also measured. As shown in Figure 1D, less than 5% cumulative CPT release was observed in the absence of DTT or in the presence of 2 μM DTT after 94 h incubation, implying minimal drug leakage during blood circulation. The general trend is that higher DTT

dx.doi.org/10.1021/ja5105848 | J. Am. Chem. Soc. 2015, 137, 362–368

levels lead to faster release of CPT in the active form. Upon 24 h incubation with 10 mM DTT, up to ~60% cumulative CPT release in a controlled manner was achieved.

We further explored MR imaging contrast performance of **hPAs** in response to the reductive milieu. Typical T_1-weighted spin−echo MR images recorded for aqueous dispersions of **hPA-2** at varying Gd^{3+} and DTT contents were measured (Figure 2A). For small molecule *alkynyl*-DOTA(Gd), positive

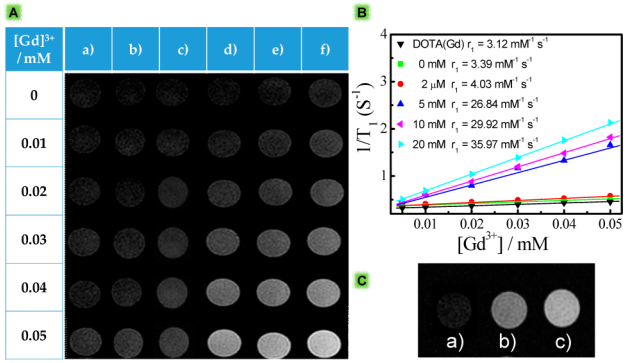

Figure 2. (A) T_1-weighted spin−echo MR images of (a) small molecule *alkynyl*-DOTA(Gd) complex and **hPA-2** after incubating with (b) 0 mM, (c) 2 μM, (d) 5 mM, (e) 10 mM, and (f) 20 mM DTT for 12 h with $[Gd^{3+}]$ in the range of 0−0.05 mM (from top to down). (B) Water proton longitudinal relaxation rates ($1/T_1$) of small-molecule *alkynyl*-DOTA(Gd) complex and **hPA-2** after treating with DTT (0−20 mM) as a function of Gd^{3+} concentrations. (C) MR images recorded for (a) untreated HepG2 cells, (b) HepG2 cells treated with **hPA-2** for 12 h, and (c) HepG2 cells pretreated with 10 mM GSH-OEt for 2 h to elevate intracellular GSH level, and then coincubated with **hPA-2** for 12 h.

contrast enhancement of MR signals was quite obvious upon elevating concentrations. When treated with DTT, **hPA**-based contrast agents in the same Gd^{3+} range exhibited substantially enhanced MR signal contrast, and higher DTT levels lead to more positive imaging contrast. Quantitative analysis was further applied (Figure 2B). Upon increasing DTT levels, T_1 relaxivity (r_1) of **hPA-2** increased from 3.39 mM^{-1} s^{-1} at 0 mM DTT to 4.03 mM^{-1} s^{-1} at 2 μM DTT (corresponding to the blood circulation condition), which were quite comparable to small molecule *alkynyl*-DOTA(Gd) (3.12 mM^{-1} s^{-1}); however, r_1 increased to 29.92 mM^{-1} s^{-1} at 10 mM DTT and even up to 35.97 mM^{-1} s^{-1} at 20 mM DTT. Thus, ~9.6-fold enhancement in T_1 relaxivity was obtained for **hPA-2** unimolecular micelles at 10 mM DTT relative to that of *alkynyl*-DOTA(Gd), and ~7.4-fold improvement compared to that under simulated blood circulation condition.

Before reductive milieu-responsive CPT release, Gd complex was located within hydrophobic and hyperbranched cores with their local rotational mobility being greatly restricted. This will considerably affect the exchange between bulk and bound water molecules surrounding Gd complex and counteract the positive contribution from the enrichment of Gd complex within hyperbranched cores. On the other hand, the core hydrophobicity mainly originate from CPTM residues, thus upon cytosol reductive milieu-triggered CPT release, the hyperbranched cores were subjected to hydrophobic-to-hydrophilic transition and became water-swollen (Scheme 2B). Thus, upon increasing DTT levels, prominent enhancement of relaxation rate occurred. Since triggered CPT release was synchronously associated with MR contrast enhancement, multifunctional **hPAs** can serve as MR-image guided self-reporting drug delivery nanocarriers. Next, reductive milieu-responsive MR contrast turn-on was confirmed by cellular MR imaging experiments upon incubating HepG2 cells with **hPA-2** (Figure 2C). Compared to the untreated control, better cellular MR contrast was observed for cells upon **hPA-2** internalization. In addition, HepG2 cells pretreated with GSH-OEt to increase the intracellular GSH level displayed more positive contrast, further verifying the activation of MR contrast in response to tumor intracellular reductive milieu for **hPAs**.

Since cellular uptake of polymeric nanocarriers follows diverse pathways, which considerably affects their destination and the final fate.[19] Guanidine residues are known to enhance cellular internalization potency of nanocarriers regardless of the scaffold.[20] Thus, cellular uptake of guanidine-decorated **hPA-2** was examined in detail against HepG2 cells by confocal laser scanning microscopy (CLSM), using guanidine-free **hPA-3** as a control. The uptake kinetics was quantified by the evolution of fluorescence intensity and localization of blue-emitting CPT emission channel. Late endosomes and lysosomes were stained with LysoTracker Red (Figure 3A). Upon co-incubation with **hPA-2** for 2 h, substantial cellular uptake into HepG2 cells was observed, exhibiting a low colocalization ratio (~30%) between blue CPT emission and LysoTracker Red-stained endolysosomes. Extending the incubation time to 4 h, cellular uptake to a higher extent was observed with stronger blue emission in the cytosol. At 12 h incubation, quite intense blue emission was observed within the whole nucleus/cytoplasm region. This confirmed effective CPT cleavage from hyperbranched cores and occurrence of nuclear drug accumulation.[11]

For guanidine-free **hPA-3**, upon 4 h co-incubation, the much weaker CPT blue emission mainly colocalized with LysoTracker Red, suggesting that **hPA-3** was mostly retained within endolysosomes. Even after 12 h incubation, nuclear CPT accumulation can be barely discerned and the colocalization ratio was ~53% (Supporting Information, Figure S4). Thus, compared to guanidine-free **hPA-3**, the presence of guanidine residues within micellar coronas in **hPA-2** contributed to faster cellular uptake and endosomal escape (Figure S4 vs Figure 3A), and this was further verified by flow cytometry results (Supporting Information, Figure S5).[21] To further probe the effect of guanidine modification on endocytic pathways involved in the cellular uptake of **hPAs**, zeta potential measurements were conducted at different pH (Figure 3B). Guanidine-free **hPA-3** was slightly negatively charged within the measured pH range. However, guanidine-decorated **hPA-2** unimolecular micelles were only slightly positively charged below pH 7.4 (0−6 mV). It seems that the random copolymerization of long side chain OEGMA monomer with GPMA and the low GPMA content (~20 mol%) can efficiently screen overall positive charges at micellar coronas, but without the loss of cellular internalization potency.

Moreover, endocytosis inhibition experiments using various potent biochemical inhibitors were also conducted (Figure 3C).[22] NaN_3/2-deoxyglucose (NaN_3/DOG) was employed to inhibit the energy-dependent pathway, resulting in a more obvious reduction in the cellular uptake of guanidine-free **hPA-3** compared with that of guanidine-decorated **hPA-2** (~83% vs ~46%), suggesting a possible energy-independent pathway for **hPA-2** uptake. The cellular penetration potency of guanidine-decorated **hPA-2** was further verified by CLSM (Figure 3D). Upon 1 h incubation with **hPA-2** in the presence of NaN_3/DOG, blue emission pixels were distinctly observed in the cell

dx.doi.org/10.1021/ja5105848 | J. Am. Chem. Soc. 2015, 137, 362−368

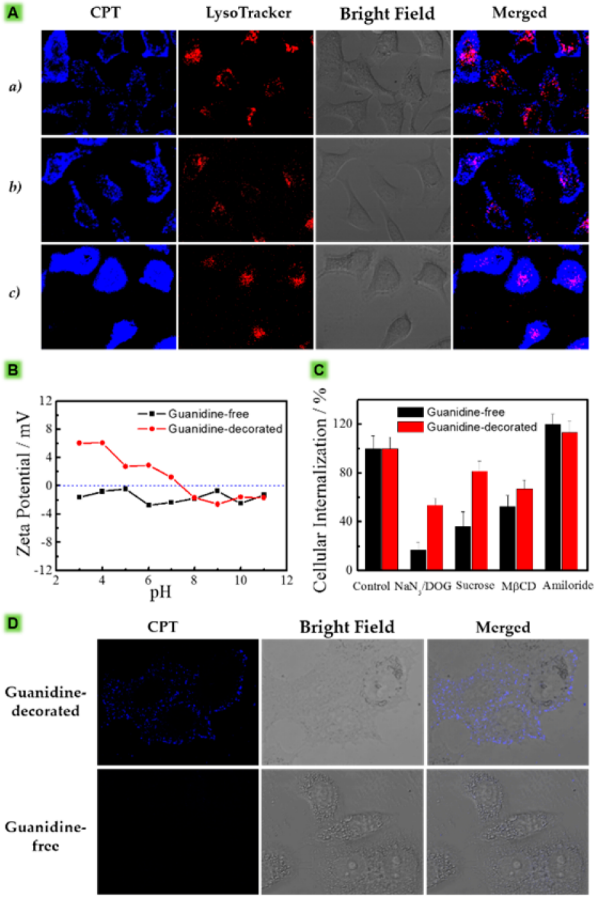

Figure 3. (A) CLSM images of HepG2 cells after coincubating with aqueous dispersion of **hPA-2** at a CPT equivalent dosage of 10 μg/mL for (a) 2 h, (b) 4 h, and (c) 12 h. Late endosomes and lysosomes were stained with LysoTracker Red (red). (B) Zeta potential recorded for aqueous solutions of (●) guanidine-decorated **hPA-2** and (■) guanidine-free **hPA-3** at varying pH values. (C) Percent internalization of guanidine-decorated and guanidine-free **hPAs** normalized to **hPA** internalization in the absence of any inhibitors. Data are mean values (~200 cells, three parallel experiments, $P < 0.05$). (D) CLSM images of HepG2 cells after incubating for 1 h with guanidine-decorated or guanidine-free **hPAs** in the presence of energy-dependent endocytic inhibitors (NaN_3/DOG).

membrane; in contrast for **hPA-3**, blue emission was hardly discernible due to almost complete blocking of endocytosis. Thus, we propose that a non-endocytic internalization pathway exists for **hPA-2**.[23] Sucrose treatment of cells is known to perturb clathrin-mediated endocytosis, which caused a dramatic reduction (~63%) in the uptake of **hPA-3** against HepG2 cells, and to a much lesser extent for guanidine-decorated **hPA-2** (~19%).

In view of additional experiments with other inhibitors such as methyl-β-cyclodextrin (MβCD) and amiloride, which block caveolae-mediated endocytosis and pinocytosis, respectively, we concluded that the uptake of guanidine-free **hPA-3** mainly followed clathrin-mediated endocytosis, whereas both caveolae-mediated endocytosis and some energy-independent events are prominent pathways for guanidine-decorated **hPA-2**. Thus, guanidine-free **hPA-3** micelles tended to be entrapped within endolysosomes, whereas **hPA-2** exhibited low colocalization ratio with endolysosomes. This is quite favorable considering that the cytosol milieu possesses the desired reductive microenvironment for triggered CPT release and turn-on of MR imaging contrast for **hPAs** (Figure 3A and Supporting Information, Figure S4).

In vitro cytotoxicity of guanidine-decorated **hPA-2** was then evaluated using MTT assay, employing guanidine-free **hPA-3** as a control. Buthionine sulfoximine (BSO) inhibitor was utilized to reduce intracellular GSH content to evaluate nanocarrier cytotoxicity under nonreductive physiological milieu. The cell viability of both guanidine-decorated and guanidine-free micelles against HepG2 cells pretreated with BSO was quite minimal, exhibiting the same level of IC_{50} values (~200.6 and ~248.3 μg mL^{-1}). This suggested that guanidine residues did not induce additional cytotoxicity toward **hPAs** (Figure 4A).

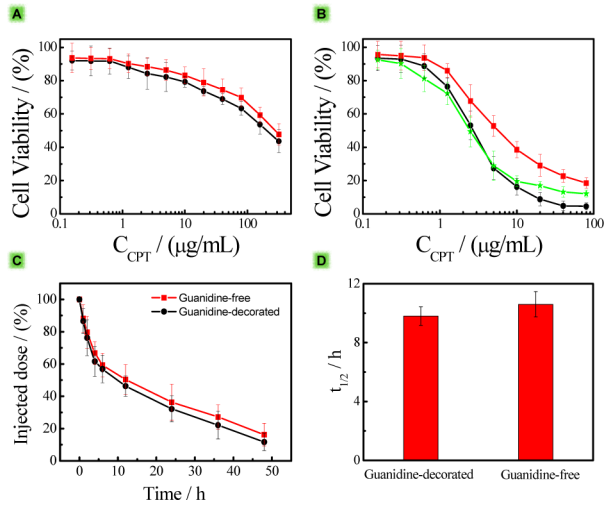

Figure 4. (A) Cell viability of HepG2 cells pretreated with 0.1 mM buthionine sulfoximine (BSO) to reduce intracellular GSH level, and then treated with **hPA-2** (●) and guanidine-free **hPA-3** (■) for 24 h. (B) Cell viability of HepG2 cells measured in the absence of BSO. Cells were treated with **hPA-2** (●), **hPA-3** (■), and CPT parent drug (★), respectively. (C) Blood level of guanidine-decorated **hPA-2** (●) and guanidine-free **hPA-3** (■) calculated as a percentage of injected doseremaining in the blood. (D) Blood circulation half-lives ($t_{1/2}$) of **hPA-2** and **hPA-3** polyprodrug unimolecular micelles. Error bars were based on three rats per group and three repetitions at each time point, $P < 0.05$.

On the contrary, in the absence of BSO, guanidine-decorated and guanidine-free **hPAs** exhibited significant differences in IC_{50}, being ~2.72 and ~5.63 μg mL^{-1}, respectively. For **hPA-2**, a 74-fold enhancement in cytotoxicity under tumor intracellular reductive milieu was observed compared to that under nonreductive physiological condition (Figure 4B).

To further confirm that reductively activated drug release within the cytosol really contributed to the observed cytotoxicity, HepG2 cells were pretreated with glutathione reduced ethyl ester (GSH-OEt) to elevate intracellular GSH levels before incubating with **hPA-2**. As shown in Supporting Information, Figure S6a, compared to the nontreated control, enhanced cytotoxicity was observed for GSH-OEt treated cells, whereas **hPA-2** exhibited negligible cytotoxicity toward BSO-treated cells (Figure 4A). In addition, in the presence of either BSO or GSH-OEt, free CPT drug exhibited similar cytotoxicity compared to the blank control (Figure S6b). The therapeutic activation of **hPA-2** can be mainly ascribed to efficient cellular penetration, reductively activated drug release in the cytosol, and considerable nuclear CPT accumulation within tumor cells.

dx.doi.org/10.1021/ja5105848 | J. Am. Chem. Soc. 2015, 137, 362−368

Moreover, during blood circulation, the therapeutic efficacy of **hPAs** was inhibited due to their nonreductive nature, which is quite desirable for nanocarriers.

In vivo blood circulation of guanidine-decorated **hPA-2** and guanidine-free **hPA-3** was then examined upon administration into healthy rats, exhibiting comparable half-lives ($t_{1/2}$) (being ~9.8 h and ~10.6 h, respectively; Figure 4C,D). It is well-recognized that prolonged blood circulation strongly affects the therapeutic efficacy of drug delivery nanocarriers. Clinical studies have suggested that circulation duration of spherical nanoparticles are generally extended by 3-fold in humans compared to those in rats.[23] Thus, we can expect long circulation times for **hPAs**, which is quite typical for branched and hyperbranched star polymers.[3a] Prominently extended blood circulation feature for **hPAs** can be ascribed to the almost neutral surface of micellar coronas and the hyperbranched chain topology with excellent chain flexibility and deformability.

CONCLUSIONS

In summary, theranostic hyperbranched polyprodrug amphiphiles, **hPAs**, were constructed with combined advantages including cell penetration potency, prolonged blood circulation, tumor intracellular reductive milieu-triggered drug release, and, most importantly, synergistic activation of therapeutic efficacy and MR imaging contrast enhancement. In aqueous media, **hPAs** exist as stable unimolecular micelles. The covalently interconnected nature endows **hPAs** with excellent structural integrity, which is a great advantage compared to conventional nanocarriers based on block copolymer micelles or vesicles. Low content of guanidine moieties randomly copolymerized within hydrophilic coronas improved the cellular penetration and uptake rate, without incurring extra cytotoxicity and sacrificing the long blood circulation feature. Controlled CPT release in the active form from polyprodrug unimolecular micelles was achieved in tumor intracellular cytosol reductive milieu, accompanied by the synergistic activation of therapeutic efficacy (>70-fold enhancement in cytotoxicity) and turn-on of MR imaging performance (~9.6-fold increase in T_1 relaxivity). We expect that the theranostic polyprodrug design based on the hyperbranched star copolymer chain topology can provide new avenues for theranostic nanocarriers in more effective and personalized cancer therapy.

ASSOCIATED CONTENT

Supporting Information

Experimental details, characterization methods, and all relevant characterization data. This material is available free of charge via the Internet at http://pubs.acs.org.

AUTHOR INFORMATION

Corresponding Author

sliu@ustc.edu.cn

Notes

The authors declare no competing financial interest.

ACKNOWLEDGMENTS

Financial support from the National Natural Scientific Foundation of China (NNSFC) Project (21274137, 51033005 and 51403042) and Specialized Research Fund for the Doctoral Program of Higher Education (SRFDP, 20123402130010) is gratefully acknowledged.

REFERENCES

(1) (a) Kataoka, K.; Harada, A.; Nagasaki, Y. *Adv. Drug Delivery Rev.* **2012**, *64*, 37−48. (b) Ge, Z. S.; Liu, S. Y. *Chem. Soc. Rev.* **2013**, *42*, 7289−7325.

(2) (a) Bannister, I.; Billingham, N. C.; Armes, S. P.; Rannard, S. P.; Findlay, P. *Macromolecules* **2006**, *39*, 7483−7492. (b) Du, W.; Li, Y.; Nyström, A. M.; Cheng, C.; Wooley, K. L. *J. Polym. Sci., Part A: Polym. Chem.* **2010**, *48*, 3487−3496. (c) Lutz, J.-F.; Sumerlin, B.; Matyjaszewski, K. *Macromol. Rapid Commun.* **2014**, *35*, 377−377. (d) Calderon, M.; Quadir, M. A.; Sharma, S. K.; Haag, R. *Adv. Mater.* **2010**, *22*, 190−218.

(3) (a) Fox, M. E.; Szoka, F. C.; Frechet, J. M. J. *Acc. Chem. Res.* **2009**, *42*, 1141−1151. (b) Li, X. J.; Qian, Y. F.; Liu, T.; Hu, X. L.; Zhang, G. Y.; You, Y. Z.; Liu, S. Y. *Biomaterials* **2011**, *32*, 6595−6605. (c) Wang, D.; Zhao, T.; Zhu, X.; Yan, D.; Wang, W. *Chem. Soc. Rev.* **2014**, DOI: 10.1039/C4CS00229F. (d) Wilms, D.; Stiriba, S.-E.; Frey, H. *Acc. Chem. Res.* **2009**, *43*, 129−141. (e) Jin, H.; Huang, W.; Zhu, X.; Zhou, Y.; Yan, D. *Chem. Soc. Rev.* **2012**, *41*, 5986−5997.

(4) Fox, M. E.; Guillaudeu, S.; Frechet, J. M. J.; Jerger, K.; Macaraeg, N.; Szoka, F. C. *Mol. Pharmaceutics* **2009**, *6*, 1562−1572.

(5) (a) Krasia-Christoforou, T.; Georgiou, T. K. *J. Mater. Chem. B* **2013**, *1*, 3002−3025. (b) Wang, Z.; Niu, G.; Chen, X. *Pharm. Res.* **2013**, 1−19.

(6) Xie, J.; Lee, S.; Chen, X. Y. *Adv. Drug Delivery Rev.* **2010**, *62*, 1064−1079.

(7) (a) Ai, H.; Flask, C.; Weinberg, B.; Shuai, X.; Pagel, M. D.; Farrell, D.; Duerk, J.; Gao, J. M. *Adv. Mater.* **2005**, *17*, 1949−1952. (b) Nasongkla, N.; Bey, E.; Ren, J. M.; Ai, H.; Khemtong, C.; Guthi, J. S.; Chin, S. F.; Sherry, A. D.; Boothman, D. A.; Gao, J. M. *Nano Lett.* **2006**, *6*, 2427−2430. (c) Mantle, M. D. *Curr. Opin. Colloid Interface Sci.* **2013**, *18*, 214−227. (d) Pourtau, L.; Oliveira, H.; Thevenot, J.; Wan, Y.; Brisson, A. R.; Sandre, O.; Miraux, S.; Thiaudiere, E.; Lecommandoux, S. *Adv. Healthcare Mater.* **2013**, *2*, 1420−1424. (e) Berret, J.-F.; Schonbeck, N.; Gazeau, F.; El Kharrat, D.; Sandre, O.; Vacher, A.; Airiau, M. *J. Am. Chem. Soc.* **2006**, *128*, 1755−1761.

(8) (a) Liu, T.; Qian, Y. F.; Hu, X. L.; Ge, Z. S.; Liu, S. Y. *J. Mater. Chem.* **2012**, *22*, 5020−5030. (b) Hu, J. M.; Qian, Y. F.; Wang, X. F.; Liu, T.; Liu, S. Y. *Langmuir* **2012**, *28*, 2073−2082. (c) Hu, J. M.; Liu, T.; Zhang, G. Y.; Jin, F.; Liu, S. Y. *Macromol. Rapid Commun.* **2013**, *34*, 749−758. (d) Ye, M. Z.; Qian, Y.; Tang, J. B.; Hu, H. J.; Sui, M. H.; Shen, Y. Q. *J. Controlled Release* **2013**, *169*, 239−245. (e) Ye, M. Z.; Tang, J. B.; Wang, X. P.; Xu, J. X.; Sui, M. H.; Shen, Y. Q. *J. Controlled Release* **2011**, *152*, 256−257. (f) Thurecht, K. J.; Blakey, I.; Peng, H.; Squires, O.; Hsu, S.; Alexander, C.; Whittaker, A. K. *J. Am. Chem. Soc.* **2010**, *132*, 5336−5337. (g) Liu, T.; Li, X. J.; Qian, Y. F.; Hu, X. L.; Liu, S. Y. *Biomaterials* **2012**, *33*, 2521−2531. (h) Li, Y.; Qian, Y. F.; Liu, T.; Zhang, G. Y.; Hu, J. M.; Liu, S. Y. *Polym. Chem.* **2014**, *5*, 1743−1750.

(9) (a) Tang, J. B.; Sheng, Y. Q.; Hu, H. J.; Shen, Y. Q. *Prog. Polym. Sci.* **2013**, *38*, 462−502. (b) Villaraza, A. J. L.; Bumb, A.; Brechbiel, M. W. *Chem. Rev.* **2010**, *110*, 2921−2959. (c) Theato, P.; Sumerlin, B. S.; O'Reilly, R. K.; Epps, I. I. I. T. H. *Chem. Soc. Rev.* **2013**, *42*, 7055−7056. (d) Major, J. L.; Meade, T. J. *Acc. Chem. Res.* **2009**, *42*, 893−903.

(10) Liu, Y. J.; Zhang, N. *Biomaterials* **2012**, *33*, 5363−5375.

(11) Hu, X. L.; Hu, J. M.; Tian, J.; Ge, Z. S.; Zhang, G. Y.; Luo, K. F.; Liu, S. Y. *J. Am. Chem. Soc.* **2013**, *135*, 17617−17629.

(12) Zhou, Z.; Ma, X.; Murphy, C. J.; Jin, E.; Sun, Q.; Shen, Y.; Van Kirk, E. A.; Murdoch, W. J. *Angew. Chem., Int. Ed.* **2014**, *53*, 10949−10955.

(13) (a) Khan, A. R.; Magnusson, J. P.; Watson, S.; Grabowska, A. M.; Wilkinson, R. W.; Alexander, C.; Pritchard, D. *Polym. Chem.* **2014**, *5*, 5320−5329. (b) Rao, N. V.; Mane, S. R.; Kishore, A.; Das Sarma, J.; Shunmugam, R. *Biomacromolecules* **2012**, *13*, 221−230. (c) Yuan, Y. Y.; Liu, J.; Liu, B. *Angew. Chem., Int. Ed.* **2014**, *53*, 7163−7168. (d) Crielaard, B. J.; Rijcken, C. J. F.; Quan, L. D.; van der Wal, S.; Altintas, I.; van der Pot, M.; Kruijtzer, J. A. W.; Liskamp, R. M. J.; Schiffelers, R. M.; van Nostrum, C. F.; Hennink, W. E.; Wang, D.; Lammers, T.; Storm, G. *Angew. Chem., Int. Ed.* **2012**, *51*, 7254−7258. (e) Johnson, J. A.; Lu, Y. Y.; Burts, A. O.; Xia, Y.; Durrell, A. C.;

Tirrell, D. A.; Grubbs, R. H. *Macromolecules* **2010**, *43*, 10326−10335. (f) Parrott, M. C.; Finniss, M.; Luft, J. C.; Pandya, A.; Gullapalli, A.; Napier, M. E.; Desimone, J. M. *J. Am. Chem. Soc.* **2012**, *134*, 7978−7982.
(14) (a) Wu, X. M.; Sun, X. R.; Guo, Z. Q.; Tang, J. B.; Shen, Y. Q.; James, T. D.; Tian, H.; Zhu, W. H. *J. Am. Chem. Soc.* **2014**, *136*, 3579−3588. (b) Bhuniya, S.; Maiti, S.; Kim, E. J.; Lee, H.; Sessler, J. L.; Hong, K. S.; Kim, J. S. *Angew. Chem., Int. Ed.* **2014**, *53*, 4469−4474. (c) Lee, M. H.; Kim, J. Y.; Han, J. H.; Bhuniya, S.; Sessler, J. L.; Kang, C.; Kim, J. S. *J. Am. Chem. Soc.* **2012**, *134*, 12668−12674.
(15) (a) Tao, L.; Liu, J. Q.; Tan, B. H.; Davis, T. P. *Macromolecules* **2009**, *42*, 4960−4962. (b) Lutz, J.-F.; Sumerlin, B.; Matyjaszewski, K. *Macromol. Rapid Commun.* **2014**, *35*, 122−122. (c) Gregory, A.; Stenzel, M. H. *Prog. Polym. Sci.* **2012**, *37*, 38−105. (d) Boyer, C.; Stenzel, M. H.; Davis, T. P. *J. Polym. Sci. Part A: Polym. Chem.* **2011**, *49*, 551−595. (e) Boyer, C.; Bulmus, V.; Davis, T. P.; Ladmiral, V.; Liu, J.; Perrier, S. *Chem. Rev.* **2009**, *109*, 5402−5436. (f) Zhang, Y.; Teo, B. M.; Postma, A.; Ercole, F.; Ogaki, R.; Zhu, M. F.; Stadler, B. *J. Phys. Chem. B* **2013**, *117*, 10504−10512. (g) Zhang, M. J.; Liu, H. H.; Shao, W.; Ye, C. N.; Zhao, Y. L. *Macromolecules* **2012**, *45*, 9312−9325. (h) Vogt, A. P.; Sumerlin, B. S. *Macromolecules* **2008**, *41*, 7368−7373. (i) Bütün, V.; Bannister, I.; Billingham, N. C.; Sherrington, D. C.; Armes, S. P. *Macromolecules* **2005**, *38*, 4977−4982.
(16) Xu, J.; Luo, S. Z.; Shi, W. F.; Liu, S. Y. *Langmuir* **2006**, *22*, 989−997.
(17) Ruiz-Sanchis, P.; Wohl, B. M.; Smith, A. A. A.; Zuwala, K.; Melchjorsen, J.; Tolstrup, M.; Zelikin, A. N. *Adv. Healthcare Mater.* **2014**, DOI: 10.1002/adhm.201400307.
(18) Kularatne, S. A.; Venkatesh, C.; Santhapuram, H. K. R.; Wang, K.; Vaitilingam, B.; Henne, W. A.; Low, P. S. *J. Med. Chem.* **2010**, *53*, 7767−7777.
(19) Canton, I.; Battaglia, G. *Chem. Soc. Rev.* **2012**, *41*, 2718−2739.
(20) (a) Wender, P. A.; Galliher, W. C.; Goun, E. A.; Jones, L. R.; Pillow, T. H. *Adv. Drug Delivery Rev.* **2008**, *60*, 452−472. (b) Lu, H.; Wang, D.; Kazane, S.; Javahishvili, T.; Tian, F.; Song, F.; Sellers, A.; Barnett, B.; Schultz, P. G. *J. Am. Chem. Soc.* **2013**, *135*, 13885−13891.
(21) Hu, X. L.; Tian, J.; Liu, T.; Zhang, G. Y.; Liu, S. Y. *Macromolecules* **2013**, *46*, 6243−6256.
(22) Gratton, S. E. A.; Ropp, P. A.; Pohlhaus, P. D.; Luft, J. C.; Madden, V. J.; Napier, M. E.; DeSimone, J. M. *Proc. Natl. Acad. Sci. U.S.A.* **2008**, *105*, 11613−11618.
(23) (a) Funhoff, A. M.; van Nostrum, C. F.; Lok, M. C.; Fretz, M. M.; Crommelin, D. J. A.; Hennink, W. E. *Bioconjugate Chem.* **2004**, *15*, 1212−1220. (b) Treat, N. J.; Smith, D.; Teng, C.; Flores, J. D.; Abel, B. A.; York, A. W.; Huang, F.; McCormick, C. L. *ACS Macro Lett.* **2011**, *1*, 100−104.